

000 054  
 001 055  
 002 056  
 003 057  
 004 058  
 005 059  
 006 060  
 007 061  
 008 062  
 009 063  
 010 064  
 011 065  
 012 066  
 013 067  
 014 068  
 015 069  
 016 070  
 017 071  
 018 072  
 019 073  
 020 074  
 021 075  
 022 076  
 023 077  
 024 078  
 025 079  
 026 080  
 027 081  
 028 082  
 029 083  
 030 084  
 031 085  
 032 086  
 033 087  
 034 088  
 035 089  
 036 090  
 037 091  
 038 092  
 039 093  
 040 094  
 041 095  
 042 096  
 043 097  
 044 098  
 045 099  
 046 100  
 047 101  
 048 102  
 049 103  
 050 104  
 051 105  
 052 106  
 053 107

## Supplementary File to “Multi-channel Weighted Nuclear Norm Minimization for Real Color Image Denoising”

Anonymous ICCV submission

Paper ID 572

In this supplementary file, we provide:

1. The proof of the Theorem 1 in the main paper.
2. More denoising results on the 24 high quality images from the Kodak PhotoCD dataset.
3. More visual comparisons of denoised images by different methods on the real noisy images of the dataset [1].
4. More visual comparisons of denoised images by different methods on the real noisy images of the dataset [2].

### 1. Proof of Theorem 1.

**Theorem 1.** Assume that the weights in  $w$  are in a non-descending order, the sequence  $\{\mathbf{X}_k\}$ ,  $\{\mathbf{Z}_k\}$ , and  $\{\mathbf{A}_k\}$  generated in Algorithm 1 satisfy:

$$(a) \lim_{k \rightarrow \infty} \|\mathbf{X}_{k+1} - \mathbf{Z}_{k+1}\|_F = 0; \quad (b) \lim_{k \rightarrow \infty} \|\mathbf{X}_{k+1} - \mathbf{X}_k\|_F = 0; \quad (c) \lim_{k \rightarrow \infty} \|\mathbf{Z}_{k+1} - \mathbf{Z}_k\|_F = 0. \quad (1)$$

*Proof.* 1. Firstly, we prove that the sequence  $\{\mathbf{A}_k\}$  generated by Algorithm 1 is upper bounded. Let  $\mathbf{X}_{k+1} + \rho_k^{-1} \mathbf{A}_k = \mathbf{U}_k \Sigma_k \mathbf{V}_k^\top$  be its singular value decomposition (SVD) [3] in the  $(k+1)$ -th iteration. According to Corollary 1 of [4], we can have the SVD of  $\mathbf{Z}_{k+1}$  as  $\mathbf{Z}_{k+1} = \mathbf{U}_k \hat{\Sigma}_k \mathbf{V}_k^\top = \mathbf{U}_k \mathcal{S}_{\frac{w}{\rho_k}}(\Sigma_k) \mathbf{V}_k^\top$ . Then we have

$$\|\mathbf{A}_{k+1}\|_F = \|\mathbf{A}_k + \rho_k (\mathbf{X}_{k+1} - \mathbf{Z}_{k+1})\|_F = \rho_k \|\rho_k^{-1} \mathbf{A}_k + \mathbf{X}_{k+1} - \mathbf{Z}_{k+1}\|_F \quad (2)$$

$$= \rho_k \|\mathbf{U}_k \Sigma_k \mathbf{V}_k^\top - \mathbf{U}_k \mathcal{S}_{\frac{w}{\rho_k}}(\Sigma_k) \mathbf{V}_k^\top\|_F = \rho_k \|\Sigma_k - \mathcal{S}_{\frac{w}{\rho_k}}(\Sigma_k)\|_F \quad (3)$$

$$= \rho_k \sqrt{\sum_i (\Sigma_k^{ii} - \mathcal{S}_{\frac{w}{\rho_k}}(\Sigma_k^{ii}))^2} \leq \rho_k \sqrt{\sum_i \left(\frac{w_i}{\rho_k}\right)^2} = \sqrt{\sum_i w_i^2}. \quad (4)$$

The inequality in the second last step can be proved as follows: given the diagonal matrix  $\Sigma_k$ , we define  $\Sigma_k^{ii}$  as the  $i$ -th element of  $\Sigma_k^{ii}$ . If  $\Sigma_k^{ii} \geq \frac{w_i}{\rho_k}$ , we have  $\mathcal{S}_{\frac{w}{\rho_k}}(\Sigma_k^{ii}) = \Sigma_k^{ii} - \frac{w_i}{\rho_k} \geq 0$ . If  $\Sigma_k^{ii} < \frac{w_i}{\rho_k}$ , we have  $\mathcal{S}_{\frac{w}{\rho_k}}(\Sigma_k^{ii}) = 0 < \Sigma_k^{ii} + \frac{w_i}{\rho_k}$ . After all, we have  $|\Sigma_k^{ii} - \mathcal{S}_{\frac{w}{\rho_k}}(\Sigma_k^{ii})| \leq \frac{w_i}{\rho_k}$  and hence the inequality holds true. Hence, the sequence  $\{\mathbf{A}_k\}$  is upper bounded.

2. Secondly, we prove that the sequence of Lagrangian function  $\{\mathcal{L}(\mathbf{X}_{k+1}, \mathbf{Z}_{k+1}, \mathbf{A}_k, \rho_k)\}$  is also upper bounded. Since the global optimal solution of  $\mathbf{X}$  and  $\mathbf{Z}$  in corresponding subproblems, we always have  $\mathcal{L}(\mathbf{X}_{k+1}, \mathbf{Z}_{k+1}, \mathbf{A}_k, \rho_k) \leq \mathcal{L}(\mathbf{X}_k, \mathbf{Z}_k, \mathbf{A}_k, \rho_k)$ . Based on the updating rule that  $\mathbf{A}_{k+1} = \mathbf{A}_k + \rho_k (\mathbf{X}_{k+1} - \mathbf{Z}_{k+1})$ , we have  $\mathcal{L}(\mathbf{X}_{k+1}, \mathbf{Z}_{k+1}, \mathbf{A}_{k+1}, \rho_{k+1}) = \mathcal{L}(\mathbf{X}_{k+1}, \mathbf{Z}_{k+1}, \mathbf{A}_k, \rho_k) + \langle \mathbf{A}_{k+1} - \mathbf{A}_k, \mathbf{X}_{k+1} - \mathbf{Z}_{k+1} \rangle + \frac{\rho_{k+1} - \rho_k}{2} \|\mathbf{X}_{k+1} - \mathbf{Z}_{k+1}\|_F^2 = \mathcal{L}(\mathbf{X}_{k+1}, \mathbf{Z}_{k+1}, \mathbf{A}_k, \rho_k) + \frac{\rho_{k+1} + \rho_k}{2\rho_k^2} \|\mathbf{A}_{k+1} - \mathbf{A}_k\|_F^2$ . Since the sequence  $\{\|\mathbf{A}_k\|_F\}$  is upper bounded, the sequence  $\{\|\mathbf{A}_{k+1} - \mathbf{A}_k\|_F\}$  is also upper bounded. Denote by  $a$  the upper bound of  $\{\|\mathbf{A}_{k+1} - \mathbf{A}_k\|_F\}$ , we have  $\mathcal{L}(\mathbf{X}_{k+1}, \mathbf{Z}_{k+1}, \mathbf{A}_{k+1}, \rho_{k+1}) \leq \mathcal{L}(\mathbf{X}_1, \mathbf{Z}_1, \mathbf{A}_0, \rho_0) + a \sum_{k=0}^{\infty} \frac{\rho_{k+1} + \rho_k}{2\rho_k^2} = \mathcal{L}(\mathbf{X}_1, \mathbf{Z}_1, \mathbf{A}_0, \rho_0) + a \sum_{k=0}^{\infty} \frac{\mu+1}{2\mu^k \rho_0} \leq \mathcal{L}(\mathbf{X}_1, \mathbf{Z}_1, \mathbf{A}_0, \rho_0) + \frac{a}{\rho_0} \sum_{k=0}^{\infty} \frac{1}{\mu^{k-1}}$ . The last inequality holds since  $\mu+1 < 2\mu$ . Since  $\sum_{k=0}^{\infty} \frac{1}{\mu^{k-1}} < \infty$ , the sequence of Lagrangian function  $\mathcal{L}(\mathbf{X}_{k+1}, \mathbf{Z}_{k+1}, \mathbf{A}_{k+1}, \rho_{k+1})$  is upper bound.

3. Thirdly, we prove that the sequences of  $\{\mathbf{X}_k\}$  and  $\{\mathbf{Z}_k\}$  are upper bounded. Since  $\|\mathbf{W}(\mathbf{Y} - \mathbf{X})\|_F^2 + \|\mathbf{Z}\|_{w,*} = \mathcal{L}(\mathbf{X}_k, \mathbf{Z}_k, \mathbf{A}_{k-1}, \rho_{k-1}) - \langle \mathbf{A}_k, \mathbf{X}_k - \mathbf{Z}_k \rangle - \frac{\rho_k}{2} \|\mathbf{X}_k - \mathbf{Z}_k\|_F^2 = \mathcal{L}(\mathbf{X}_k, \mathbf{Z}_k, \mathbf{A}_{k-1}, \rho_{k-1}) + \frac{1}{2\rho_k} (\|\mathbf{A}_{k-1}\|_F^2 - \|\mathbf{A}_k\|_F^2)$ . Thus  $\{\mathbf{W}(\mathbf{Y} - \mathbf{X}_k)\}$  and  $\{\mathbf{Z}_k\}$  are upper bounded, and hence the sequence  $\{\mathbf{X}_k\}$  is bounded by the Cauchy-Schwarz inequality

Table 1. PSNR(dB) results of different denoising methods on 24 natural images.

Image#	$\sigma_r = 5, \sigma_g = 30, \sigma_b = 15$								
	CBM3D	MLP	TNRD	NI	NC	WNNM-1	WNNM-2	WNNM-3	MC-WNNM
1	27.25	28.06	28.62	25.00	29.55				
2	29.70	31.30	32.70	27.80	29.69				
3	30.34	31.98	34.07	28.02	31.93				
4	29.47	31.10	32.56	27.70	32.56				
5	27.31	28.59	29.35	26.14	30.00				
6	28.20	29.10	29.90	26.15	28.81				
7	29.73	31.60	33.46	27.22	31.63				
8	27.47	28.16	28.91	25.34	30.16				
9	30.07	31.63	33.55	27.86	31.54				
10	29.96	31.37	33.20	27.74	33.44				
11	28.73	29.85	30.87	26.98	30.16				
12	30.20	31.50	33.31	27.97	31.69				
13	26.18	26.69	26.98	25.14	27.97				
14	27.86	29.07	29.87	26.67	29.21				
15	29.91	31.58	33.13	28.04	31.17				
16	29.29	30.35	31.54	27.46	32.18				
17	29.50	31.09	32.52	27.81	32.80				
18	27.72	28.74	29.36	26.57	28.63				
19	28.98	30.18	31.35	27.25	29.79				
20	30.63	31.78	33.27	27.89	29.52				
21	28.50	29.58	30.54	26.86	31.71				
22	28.61	29.78	30.82	27.19	30.50				
23	30.60	32.66	35.06	28.17	32.82				
24	27.97	28.81	29.61	26.01	30.75				
<b>Average</b>	28.92	30.19	31.44	27.04	30.76	31.89			

and triangle inequality. We can obtain that  $\lim_{k \rightarrow \infty} \|\mathbf{X}_{k+1} - \mathbf{Z}_{k+1}\|_F = \lim_{k \rightarrow \infty} \rho_k^{-1} \|\mathbf{A}_{k+1} - \mathbf{A}_k\|_F = 0$  and the equation (a) is proved.

4. Then we can prove that  $\lim_{k \rightarrow \infty} \|\mathbf{X}_{k+1} - \mathbf{X}_k\|_F = \lim_{k \rightarrow \infty} \|(\mathbf{W}^\top \mathbf{W} + \frac{\rho_k}{2} \mathbf{I})^{-1} (\mathbf{W}^\top \mathbf{WY} - \mathbf{W}^\top \mathbf{WZ}_k - \frac{1}{2} \mathbf{A}_k) - \rho_k^{-1} (\mathbf{A}_k - \mathbf{A}_{k-1})\|_F \leq \lim_{k \rightarrow \infty} \|(\mathbf{W}^\top \mathbf{W} + \frac{\rho_k}{2} \mathbf{I})^{-1} (\mathbf{W}^\top \mathbf{WY} - \mathbf{W}^\top \mathbf{WZ}_k - \frac{1}{2} \mathbf{A}_k)\|_F + \rho_k^{-1} \|\mathbf{A}_k - \mathbf{A}_{k-1}\|_F = 0$  and hence (b) is proved.

5. Finally, (c) can be proved by checking that  $\lim_{k \rightarrow \infty} \|\mathbf{Z}_{k+1} - \mathbf{Z}_k\|_F = \lim_{k \rightarrow \infty} \|\mathbf{X}_k + \rho_k^{-1} \mathbf{A}_{k-1} - \mathbf{Z}_k + \mathbf{X}_{k+1} - \mathbf{X}_k + \rho_k^{-1} \mathbf{A}_{k-1} + \rho_k^{-1} \mathbf{A}_k - \rho_k^{-1} \mathbf{A}_{k+1}\|_F \leq \lim_{k \rightarrow \infty} \|\Sigma_{k-1} - \mathcal{S}_{w/\rho_{k-1}}(\Sigma_{k-1})\|_F + \|\mathbf{X}_{k+1} - \mathbf{X}_k\|_F + \rho_k^{-1} \|\mathbf{A}_{k-1} + \mathbf{A}_{k+1} - \mathbf{A}_k\|_F = 0$ , where  $\mathbf{U}_{k-1} \Sigma_{k-1} \mathbf{V}_{k-1}^\top$  is the SVD of the matrix  $\mathbf{X}_k + \rho_{k-1} \mathbf{A}_{k-1}$ .  $\square$

## 2. More denoising results on the 24 high quality images from the Kodak PhotoCD dataset

In the main paper, we have given the PSNR results of the competing methods on the 24 high quality images from the Kodak PhotoCD dataset when the noise standard deviations are  $\sigma_r = 40, \sigma_g = 20, \sigma_b = 30$ . Here we provide more denoising results on this dataset. In Tables ??-??, we give more PSNR results on these images when the noise standard deviations are  $\sigma_r = 5, \sigma_g = 30, \sigma_b = 15$  in Table 1 and  $\sigma_r = 30, \sigma_g = 10, \sigma_b = 50$  in Table 2, respectively. In Figures 1-??, we give the visual comparisons of the denoised images by different methods.

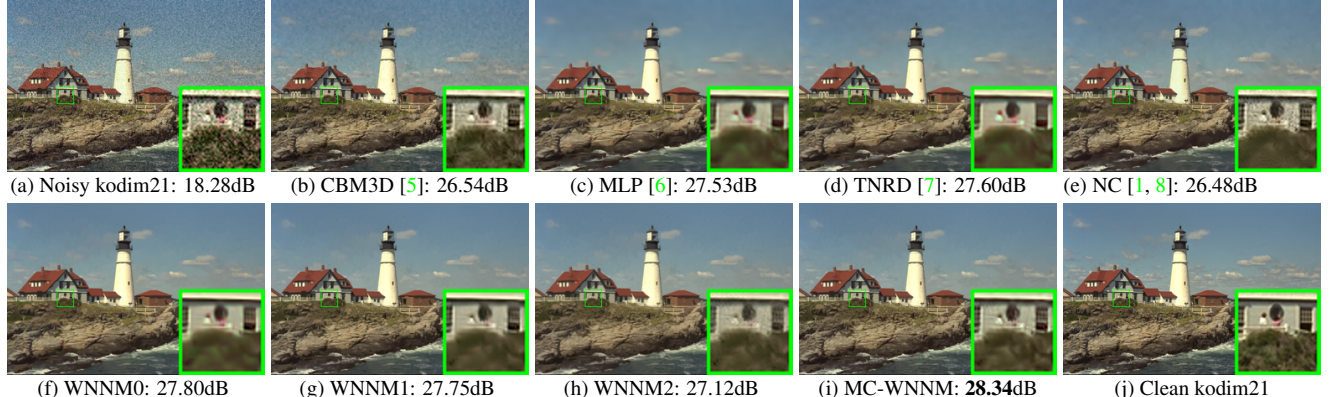
Fig. 1 shows a scene denoised by the compared methods. We can see that the methods of CBM3D and NC would remain some noise on the recovered images. The methods of MLP, TNRD, and “WNNM0”, which process separately the channels of color images, would over-smooth the images and generate false colors or artifacts. The method “WNNM1”, which process jointly the channels of color images, would not generate false colors, but still over-smooth the image. The “WNNM2”, which is the WNNM model solved by ADMM algorithm, would remain some noise on the image. By employing the proposed MC-WNNM model, our method preserves the structures (e.g., textures in windows and grass) better across the R, G, B channels and generate less artifacts than other denoising methods, leading to visually pleasant outputs.

## 3. More visual comparisons of denoised images by different methods on the real noisy images of the dataset [1]

In this section, we give more comparisons of the state-of-the-art denoising methods on the dataset [1]. The real noisy images in dataset [1] have no “ground truth” images and hence we only compare the visual quality of the denoised images

Table 2. PSNR(dB) results of different denoising methods on 24 natural images.

Image#	CBM3D	MLP	TNRD	NI	NC	WNNM-1	WNNM-2	WNNM-3	MC-WNNM
1	23.38	26.49	26.50	24.82	23.59				
2	25.19	30.94	30.90	26.82	27.79				
3	25.39	32.03	32.09	27.52	27.41				
4	24.96	30.55	30.47	27.34	27.00				
5	23.29	26.65	26.73	25.72	26.67				
6	24.09	27.76	27.70	26.10	26.12				
7	24.89	30.70	30.72	27.17	28.07				
8	23.30	26.12	26.27	25.59	26.11				
9	25.20	31.35	31.31	27.74	28.33				
10	25.13	31.01	31.05	27.60	28.53				
11	24.54	28.79	28.82	26.72	24.40				
12	25.43	31.60	31.60	27.82	29.01				
13	22.50	24.71	24.73	24.96	23.36				
14	23.91	27.69	27.72	26.26	23.08				
15	25.45	31.09	31.05	27.36	28.49				
16	24.89	29.79	29.73	27.35	27.10				
17	25.12	30.26	30.24	27.15	27.54				
18	23.83	27.26	27.26	26.05	26.15				
19	24.63	29.40	29.39	27.06	27.41				
20	26.43	31.16	31.27	26.43	26.92				
21	24.24	28.26	28.27	26.66	27.18				
22	24.51	29.03	29.06	26.83	27.64				
23	25.55	32.87	32.75	27.60	23.75				
24	23.85	27.06	27.13	25.86	27.05				
<b>Average</b>	24.57	29.27	29.28	26.69	26.61				

Figure 1. Denoised images of different methods on the image “kodim21” degraded by AWGN with different standard derivations of  $\sigma_r = 40, \sigma_g = 20, \sigma_b = 30$  on R, G, B channels, respectively. The images are better to be zoomed in on screen.

by different methods. As can be seen from Figures 2-5, our proposed method performs better than the competing methods.

#### 4. More visual comparisons of denoised images by different methods on the real noisy images of the dataset [2]

In this section, we provide more comparisons of the proposed method with the state-of-the-art denoising methods on the 15 cropped real noisy images used in [2]. In this dataset, each scene was shot 500 times under the same camera and camera setting. The mean image of the 500 shots is roughly taken as the “ground truth”, with which the PSNR can be computed. As can be seen from Figures 6-10, in most cases, our proposed method achieves better performance than the the competing methods. This validates the effectiveness of our proposed external prior guided internal prior learning framework for real noisy image denoising.

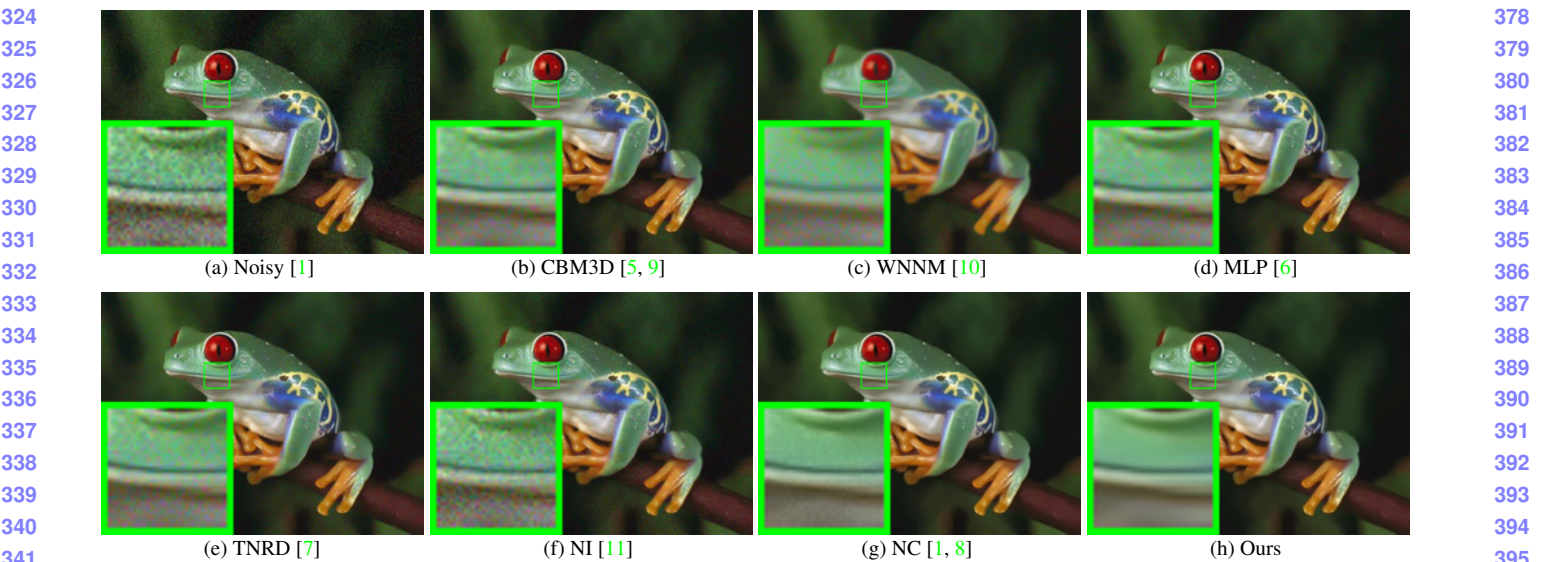


Figure 2. Denoised images of the real noisy image “Frog” [1] by different methods. The images are better to be zoomed in on screen.

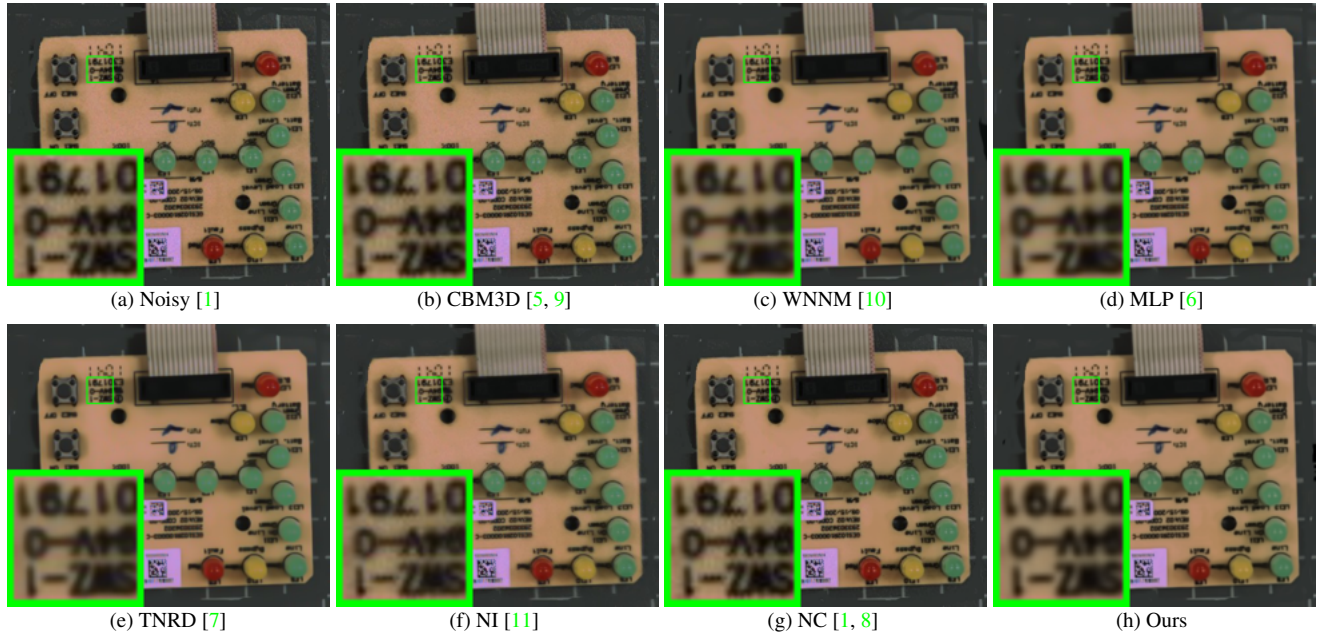
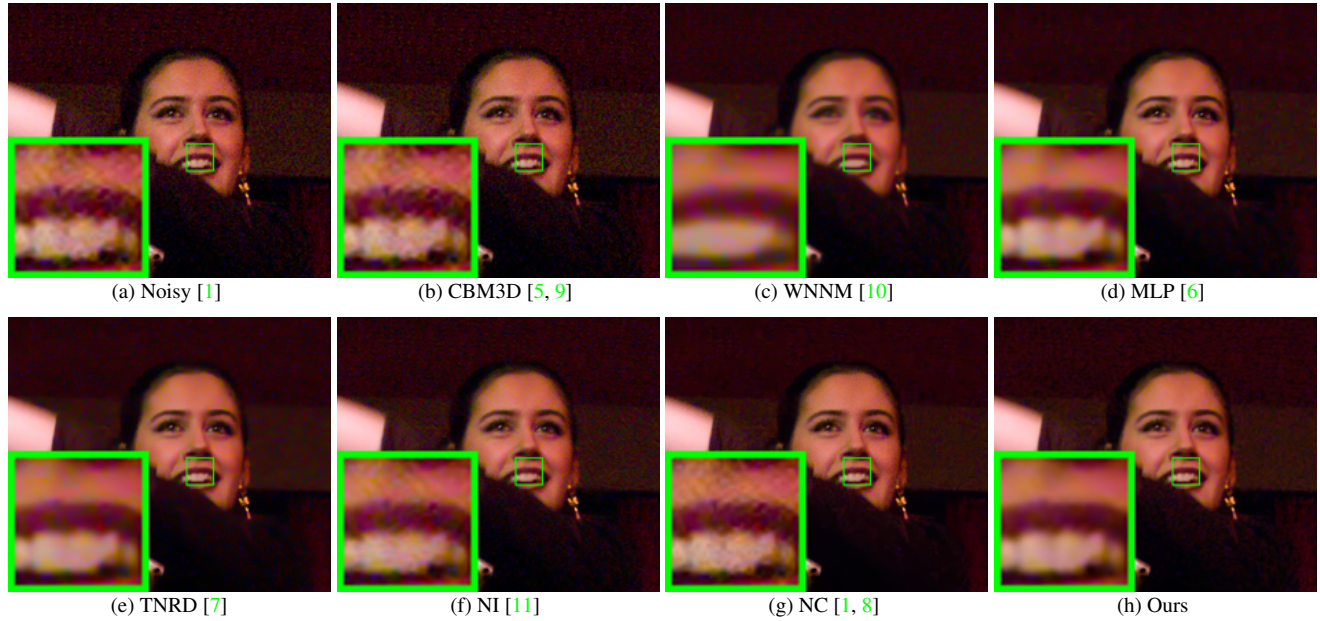


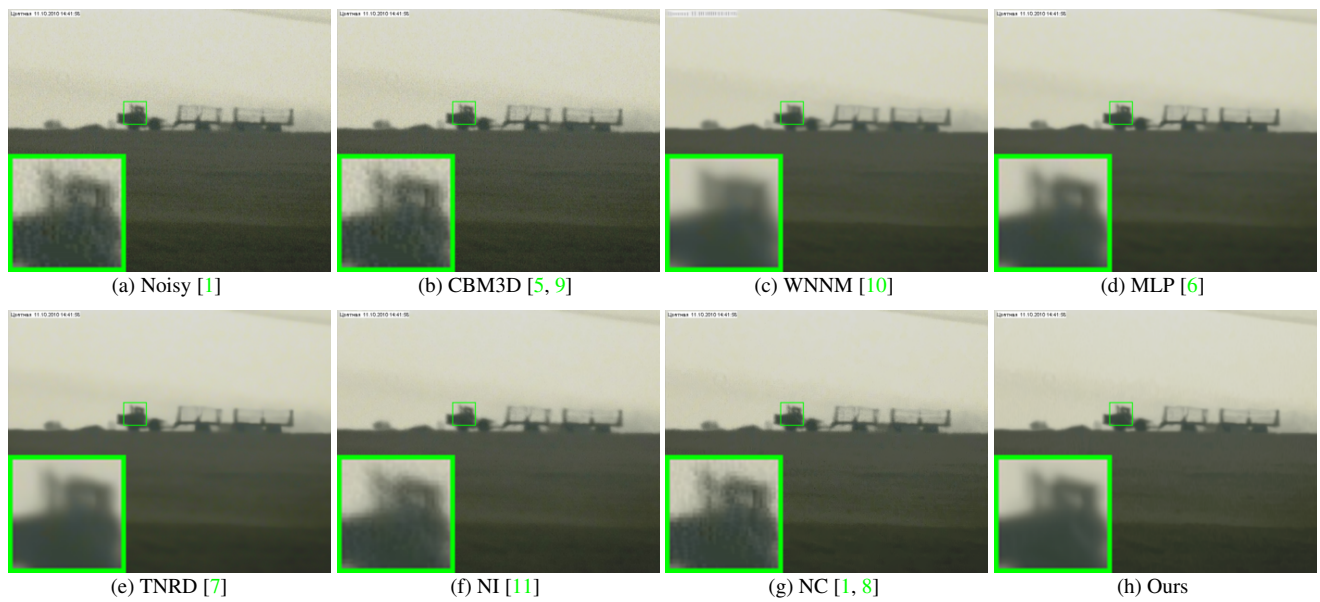
Figure 3. Denoised images of the real noisy image “Circuit” [1] by different methods. The images are better to be zoomed in on screen.

## References

- [1] M. Lebrun, M. Colom, and J. M. Morel. The noise clinic: a blind image denoising algorithm. <http://www.ipol.im/pub/art/2015/125/>. Accessed 01 28, 2015. 1, 2, 3, 4, 5, 6, 7, 8
- [2] S. Nam, Y. Hwang, Y. Matsushita, and S. J. Kim. A holistic approach to cross-channel image noise modeling and its application to image denoising. *IEEE Conference on Computer Vision and Pattern Recognition (CVPR)*, pages 1683–1691, 2016. 1, 3, 6, 7, 8
- [3] C. Eckart and G. Young. The approximation of one matrix by another of lower rank. *Psychometrika*, 1(3):211–218, 1936. 1
- [4] S. Gu, Q. Xie, D. Meng, W. Zuo, X. Feng, and L. Zhang. Weighted nuclear norm minimization and its applications to low level vision. *International Journal of Computer Vision*, pages 1–26, 2016. 1
- [5] K. Dabov, A. Foi, V. Katkovnik, and K. Egiazarian. Color image denoising via sparse 3D collaborative filtering with grouping

432  
433  
434  
435  
436  
437  
438  
439  
440  
441442  
443  
444  
445  
446  
447  
448  
449  
450  
451452 Figure 4. Denoised images of the real noisy image “Woman” [1] by different methods. The images are better to be zoomed in on screen.  
453

454



455

456 Figure 5. Denoised images of the real noisy image “Vehicle” [1] by different methods. The images are better to be zoomed in on screen.  
457

458

487 constraint in luminance-chrominance space. *IEEE International Conference on Image Processing (ICIP)*, pages 313–316, 2007. 3,  
4, 5, 6, 7, 8

488

[6] H. C. Burger, C. J. Schuler, and S. Harmeling. Image denoising: Can plain neural networks compete with BM3D? *IEEE Conference*  
489 *on Computer Vision and Pattern Recognition (CVPR)*, pages 2392–2399, 2012. 3, 4, 5, 6, 7, 8

490

[7] Y. Chen, W. Yu, and T. Pock. On learning optimized reaction diffusion processes for effective image restoration. *IEEE Conference*  
491 *on Computer Vision and Pattern Recognition (CVPR)*, pages 5261–5269, 2015. 3, 4, 5, 6, 7, 8

492

[8] M. Lebrun, M. Colom, and J.-M. Morel. Multiscale image blind denoising. *IEEE Transactions on Image Processing*, 24(10):3149–  
493 3161, 2015. 3, 4, 5, 6, 7, 8

494

495  
496  
497  
498  
499  
500  
501  
502  
503  
504  
505  
506  
507  
508  
509  
510  
511  
512  
513  
514  
515  
516  
517  
518  
519  
520  
521  
522  
523  
524  
525  
526  
527  
528  
529  
530  
531  
532  
533  
534  
535  
536  
537  
538  
539

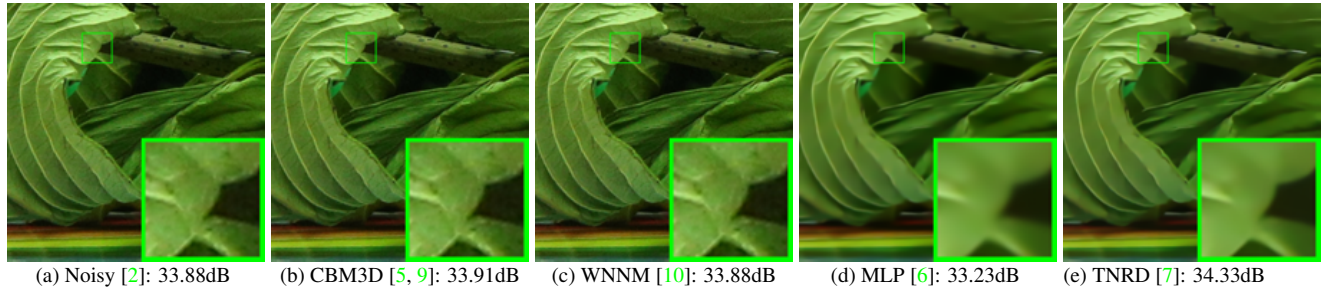
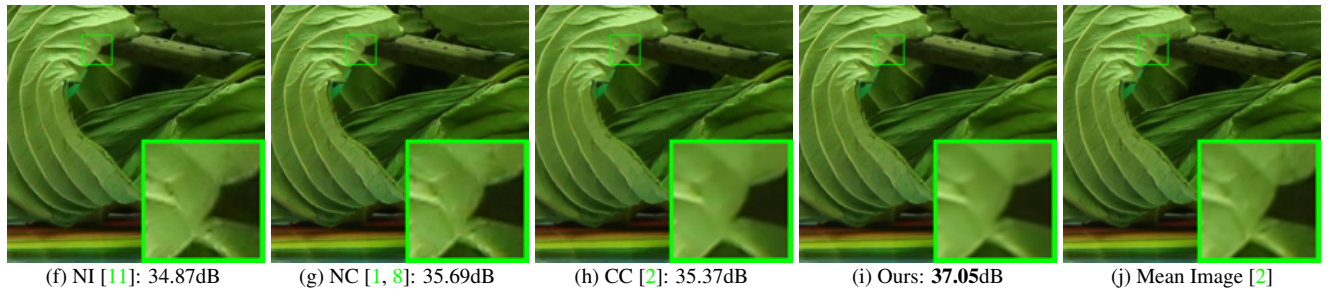
540  
541  
542  
543  
544  
545  
546  
547  
548  
549594  
595  
596  
597  
598  
599  
600  
601  
602  
603550  
551  
552  
553  
554  
555  
556  
557  
558604  
605  
606  
607  
608  
609  
610  
611  
612  
613  
614  
615

Figure 6. Denoised images of a region cropped from the real noisy image “Canon 5D Mark 3 ISO 3200 2” [2] by different methods. The images are better to be zoomed in on screen.

561

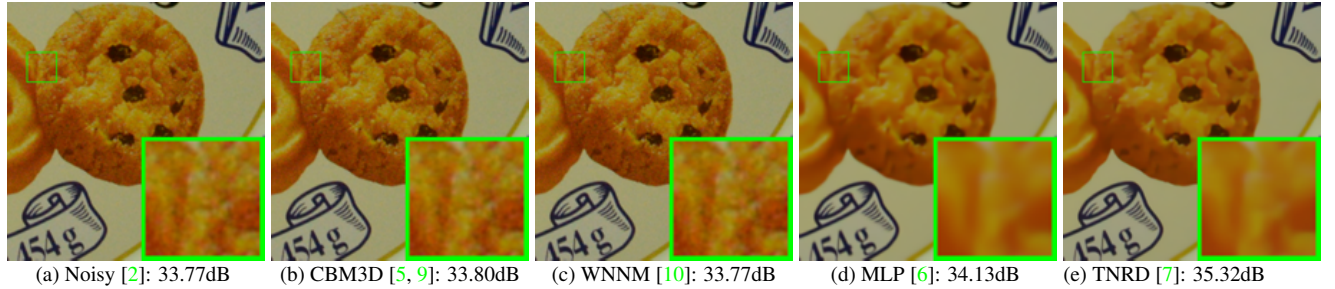
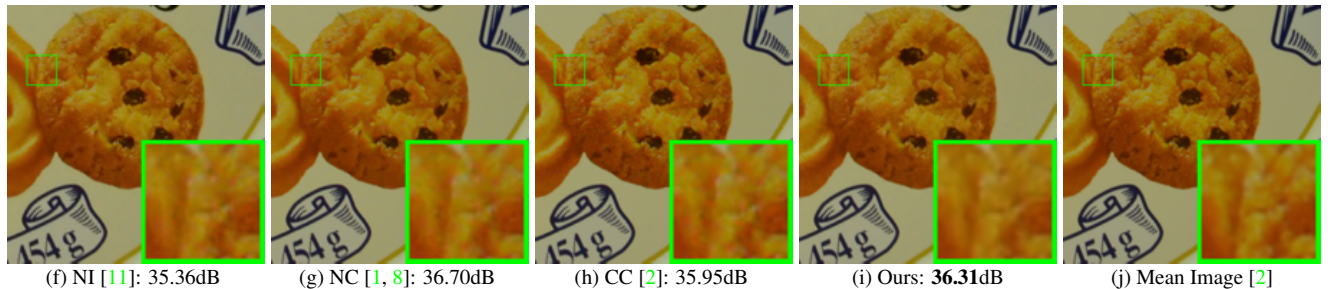
616  
617  
618  
619  
620  
621  
622  
623  
624  
625626  
627  
628  
629  
630  
631  
632  
633  
634

Figure 7. Denoised images of a region cropped from the real noisy image “Nikon D600 ISO 3200 2” [2] by different methods. The images are better to be zoomed in on screen.

583

- [9] K. Dabov, A. Foi, V. Katkovnik, and K. Egiazarian. Image denoising by sparse 3-D transform-domain collaborative filtering. *IEEE Transactions on Image Processing*, 16(8):2080–2095, 2007.
- [10] S. Gu, L. Zhang, W. Zuo, and X. Feng. Weighted nuclear norm minimization with application to image denoising. *IEEE Conference on Computer Vision and Pattern Recognition (CVPR)*, pages 2862–2869, 2014.
- [11] Neatlab ABSoft. Neat Image. <https://ni.neatvideo.com/home>.

638  
639  
640  
641  
642  
643  
644  
645  
646  
647

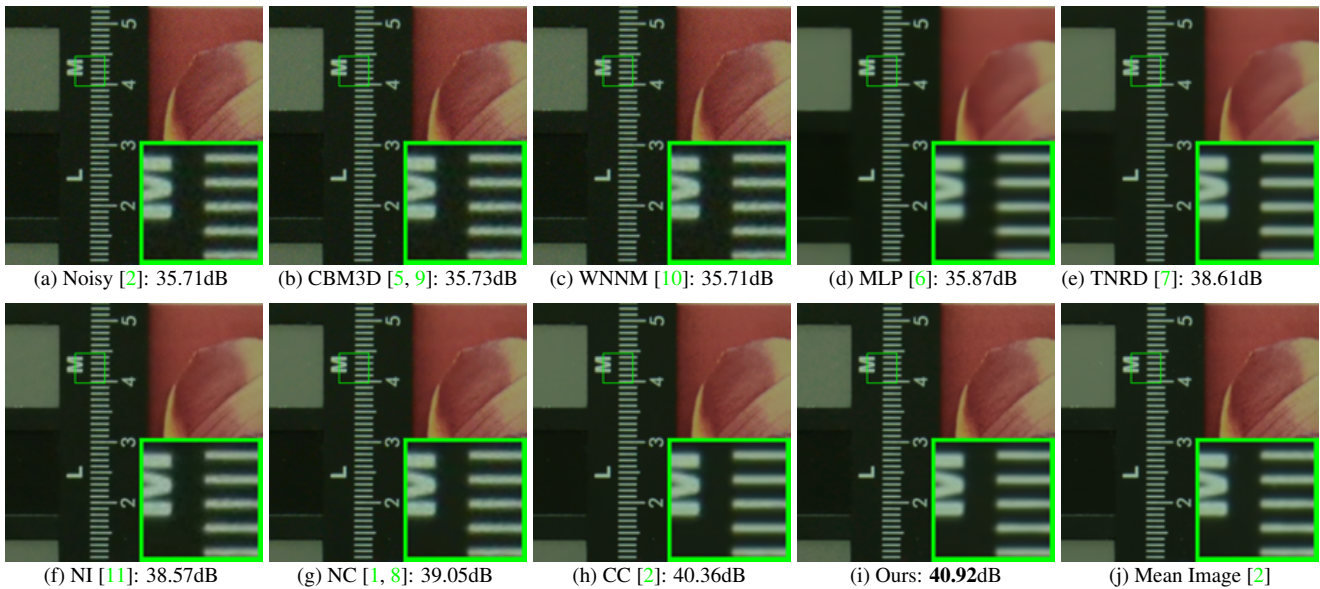


Figure 8. Denoised images of a region cropped from the real noisy image “Nikon D800 ISO 1600 2” [2] by different methods. The images are better to be zoomed in on screen.

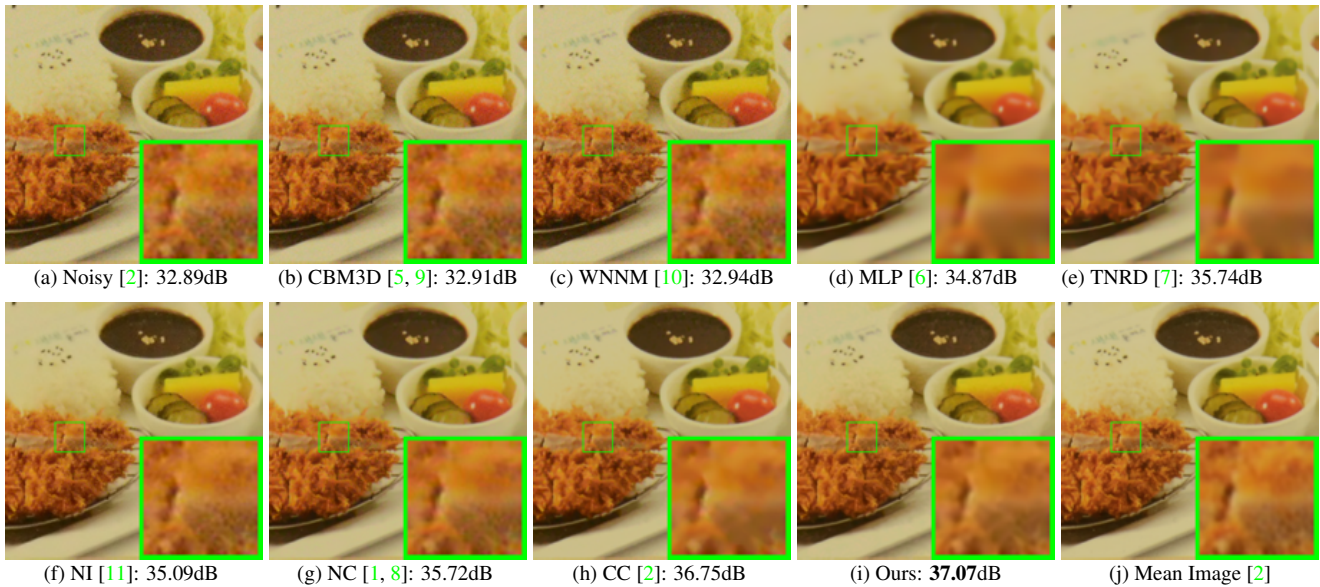


Figure 9. Denoised images of a region cropped from the real noisy image “Nikon D800 ISO 3200 2” [2] by different methods. The images are better to be zoomed in on screen.

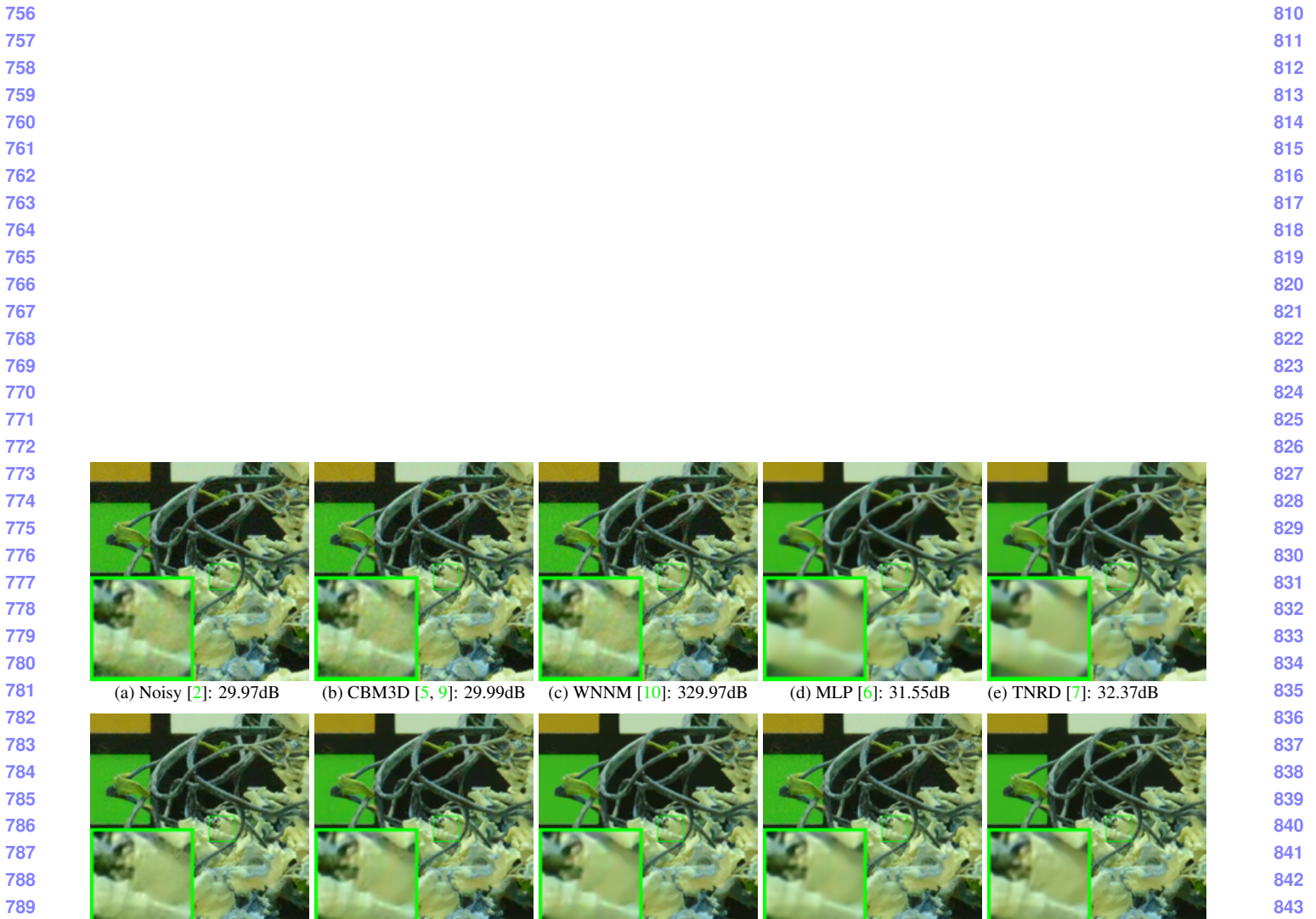


Figure 10. Denoised images of a region cropped from the real noisy image “Nikon D800 ISO 6400 2” [2] by different methods. The images are better to be zoomed in on screen.